THE JOURNAL OF PHYSICAL CHEMISTRY A

Article

pubs.acs.org/JPCA

CASPT2 Study of Photodissociation Pathways of Ketene

Hongyan Xiao,[†] Satoshi Maeda,*[,‡] and Keiji Morokuma*[,†,§]

[†]Fukui Institute for Fundamental Chemistry, Kyoto University, 34-4 Takano Nishihiraki-cho, Sakyo, Kyoto 606-8103, Japan

[‡]Department of Chemistry, Faculty of Science, Hokkaido University, Sapporo, 060-0810, Japan

[§]Cherry L. Emerson Center for Scientific Computation and Department of Chemistry, Emory University, Atlanta, Georgia 30322, United States

Supporting Information

ABSTRACT: The mechanism of various photodissociation channels of ketene involving the three lowest singlet states (S_0, S_1, and S_2) and the three lowest triplet states (T_1, T_2, and T_3) was investigated by means of the (MS-)CAS(8e,8o)PT2/6-31+G* method. Stationary structures, i.e., global minima (GMs), local minima (LMs), transition states (TSs), minimum energy conical intersections (MECIs), and minima on seam of crossing (MSXs), were explored systematically by the global reaction route mapping (GRRM) strategy. On the basis of these structures, we discussed related dissociation channels starting from S_2 that have been studied experimentally with 193−215 nm excitation wavelength. Five working pathways were found for relaxation to the low-lying S_0, S_1, and T_1 potential energy surfaces (PESs) from the Franck−Condon region of S_2, and the relaxation is expected to occur very quickly. On these low-lying states, five dissociation channels are open: three CH_2 + CO channels for different CH_2 electronic states, H + HCCO, and H_2 + C_2O. Pathways for all of these five channels were identified and discussed, including new minor paths leading to H_2 + C_2O.

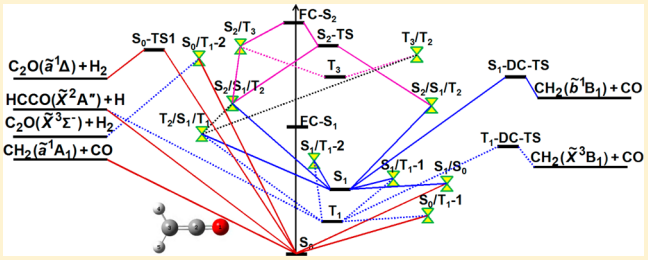

1. INTRODUCTION

The photodissociation dynamics of ketene (H_2CCO) has been studied extensively both experimentally[1−11] and theoretically[12−25] in the past several decades. Experimentally, the following five channels have been studied so far.

$$H_2CCO + h\nu \rightarrow CH_2(\tilde{X}^3B_1) + CO \quad (1)$$

$$CH_2(\tilde{a}^1A_1) + CO \quad (2)$$

$$CH_2(\tilde{b}^1B_1) + CO \quad (3)$$

$$HCCO(\tilde{X}^2A'') + H \quad (4)$$

$$C_2O + H_2 \quad (5)$$

In the near-ultraviolet absorption region (300−360 nm), the mechanism has been understood well both experimentally and theoretically.[1−4,7,16−19,21−25] H_2CCO is excited to the first excited singlet state (S_1), then undergoes a nonadiabatic transition to the lower electronic state, i.e., the ground singlet state (S_0) or the ground triplet state (T_1), and finally dissociates to CH_2 and CO with the C═C bond fission on either S_0 or T_1, which correspond to pathway 2 and pathway 1, respectively.

The higher excitation energy regions (193−215 nm), involving the second excited singlet state (S_2), have also been studied experimentally. Liu et al.[5] examined the $^1B_1$ (S_2) state photodissociation dynamics by far-ultraviolet resonance Raman spectroscopy with 217 and 200 nm excitations and indicated that the initial dynamics proceeds along the C_s-I mode in which the CCO skeleton bends out of the molecular plane. Glass et al.[8] studied the photolysis at 193 nm by atomic resonance absorption spectroscopy and revealed that the quantum yield of pathway 1 (0.628) is larger than that of pathway 2 (0.193). Feltham et al.[9] investigated the kinetic energy and angular distributions of H atom products with a 193−215 nm range by H Rydberg atom photofragment translational spectroscopy and suggested that the dissociation occurs on S_0 after a series of internal conversions (ICs) from the $^1B_1$ (S_2) state. Yang and co-workers[10] reported the photodissociation dynamics at 208 and 213 nm using the velocity map ion-imaging, and the rotational propensity of angular anisotropy observed was interpreted as the dynamical influence of a peculiar conical intersection (CI) between the $^1B_1$ (S_2) and $^1A_2$ (S_1) states along the C_s-I mode. In contrast to the results by Glass et al.,[8] Fockenberg[11] showed that a decomposition to the singlet-state CH_2 and CO is the main channel at 193.3 nm using a time-of-flight mass spectrometer. However, whether methylene is initially produced in the $^1B_1$ or $^1A_1$ state remains unclear.

In comparison with numerous experimental explorations, theoretical studies on processes that require high excess energy are limited. As early as in 1978, Yamabe and Morokuma reported state correlation diagrams for all pertinent dissociation

Special Issue: Joel M. Bowman Festschrift

Received: December 24, 2012
Revised: January 31, 2013
Published: February 2, 2013

   dx.doi.org/10.1021/jp312719a | J. Phys. Chem. A 2013, 117, 7001−7008

channels by STO-3G SCF level of theory.[12] Allen and Schaefer investigated the potential energy surfaces (PESs) of the low-lying electronic states by SCF and CISD methods in combination with DZP basis set and predicted that the S_2 state dissociates monotonically to $CH_2(\tilde{b}^1B_1)$ + $CO(\tilde{X}^1\Sigma^+)$ along the C_s-I symmetry.[13,14] The electronic states (valence states and Rydberg states) and vertical excitation energies of ketene were reported by Szalay and co-workers using EOM-CCSD and CIS methods.[15] Liu et al.[20] proposed an IC path from S_2 to the lower singlet states on the basis of the CASPT2//CASSCF/aug-cc-pVTZ calculations.

To discuss all the above five dissociation channels comprehensively at the same computation level, we performed an extensive search for photodissociation pathways at the CASPT2 level by the global reaction route mapping (GRRM) strategy, on the six lowest electronic states (S_0, S_1, S_2, T_1, T_2, and T_3). In addition to the IC path from S_2 reported by Liu et al.,[20] four unique pathways from S_2 to S_0 involving the triplet states were located in the present search. These are proposed as alternative nonadiabatic decay pathways, supported in part by a recent argument that the intersystem crossing (ISC) can compete with IC in the close vicinity of seams of potential crossing even if spin−orbit coupling is not very strong.[26] A minor CH_2 generation path from S_1 as well as a wide seam between S_0 and T_1 along the CH_2 dissociation coordinate was also newly identified. Moreover, H_2 dissociation channels involving the three lowest states, S_0, T_1, and S_1, are explored thoroughly for the first time.

2. CALCULATION DETAILS

Global minimum (GM), local minimum (LM), transition state (TS), and minimum energy conical intersection (MECI) between states of same spin, and minimum on seam of crossing (MSX) structures between singlet and triplet on and among PESs for the six lowest electronic states (S_0, S_1, S_2, T_1, T_2, and T_3) were explored systematically at the multistate (MS-)CAS(6e,5o)PT2/6-31G level by the GRRM strategy employing the anharmonic downward distortion following (ADDF) method[27−30] in combination with the seam model function and avoiding model function approaches.[27,31] The artificial force induced reaction (AFIR) method[32] was also employed to find intramolecular recombination pathways. All obtained structures on and among the six PESs were fully reoptimized without any symmetry constraint at the (MS-)CAS(8e,8o)PT2/6-31+G* level, where reference molecular orbitals for each spin-multiplicity were obtained by the state-averaged CAS(8e,8o)-SCF/6-31+G* method with equal weights for the lowest three states. MECIs and MSXs were optimized using the direct gradient method[33] and the branching plane updating method.[34] A minimum energy path within the S_0/T_1 crossing seam (S_0/T_1-MEPX) was also calculated, as discussed later by using an algorithm described in ref 34. GMs, LMs, and TSs were validated by means of the normal-mode analysis and intrinsic reaction coordinate (IRC) calculations. These calculations were performed by the GRRM program[35] using energies and gradient vectors computed by Molpro 2006 program.[36] The dissociation energies of products were calculated by constrained optimizations at the (MS-)CAS(8e,8o)PT2/6-31+G* level, fixing an interfragment distance at 10.0 Å. The three-state averaging was employed with equal weight for the first three singlet states and the first three triplet states in the reference CASSCF calculations, respectively. The shift parameter 0.3 was applied in the MS-CASPT2 calculations to avoid the intruder-state problem.[37] Spin−orbit coupling (SO-coupling) values were computed at the CAS(8e,8o)SCF/6-31+G* level averaging three singlet and three triplet states with equal weight using the Molpro 2010 program.[38] To verify the chosen active space and basis set, some key structures were also optimized by the (MS-)CAS(10e,10o)PT2/aug-cc-pVTZ method. In addition, the vertical excitation energies (T_v) and oscillator strengths (f) were calculated at the (MS-)CAS-(10e,10o)PT2/6-311+G* and (MS-)CAS(8e,8o)PT2/6-31+G* levels employing the Molcas 7.4 program.[39] We note that in the FC region, the active space (14e,14o) includes all valence orbitals and electrons with the exception of oxygen 2s, plus the 3s Rydberg orbital. The active space (10e,10o) further excludes σ and σ^* orbitals and electrons of two C−H bonds, and the active space (8e,8o) additionally excludes σ and σ^* orbitals and electrons of C−O bond.

3. RESULTS AND DISCUSSION

3.1. Photoexcitation. The vertical excitation energies T_v and oscillator strengths f were calculated and tabulated in Table 1. As shown in Table 1, T_v values for these low-lying states using different calculation levels well reproduce experimental ones. The S_2 state has relatively strong absorption with a large f value. S_2 and T_3 correspond to Rydberg states, originating from the electronic promotion from $2b_1$ to $3sa_1$ orbital ($2b_1 \rightarrow 3sa_1$). The S_1 and T_1 states are valence states with a $\pi_\perp \rightarrow \pi_\parallel^*$ ($\perp$ and $\parallel$ denote molecular orbital out of the molecular plane and in the molecular plane, respectively) electronic transition, and the second excited triplet state (T_2) is also a valence state with a $\pi_\perp \rightarrow \pi_\perp^*$ electronic transition. The corresponding molecular orbitals are shown in Figure 1. In the Franck−Condon (FC) region, below S_2 there are five states, that is, S_0, S_1, T_1, T_2, and T_3. Therefore, the PESs of these six electronic states were considered in the present study.

Table 1. Vertical Excitation Energies (T_v) and Oscillator Strengths (f) in Parentheses

states	T_V (eV)[a]	T_V (eV)[b]	exp[c]	characteristic
S_0 (1^1A_1)	0	0	0	
S_1 (1^1A_2)	3.72 (0.000)	3.80 (0.000)	3.69, 3.84, 3.87	$\pi_\perp \rightarrow \pi_\parallel^*$
S_2 (1^1B_1)	5.97 (0.033)	6.01 (0.040)	5.77, 5.81, 5.86	$\pi_\perp \rightarrow$ 3s (O)
T_1 (1^3A_2)	3.62	3.72	3.35, 3.79	$\pi_\perp \rightarrow \pi_\parallel^*$
T_2 (1^3A_1)	5.42	5.53	5.00, 5.29	$\pi_\perp \rightarrow \pi_\perp^*$
T_3 (1^3B_1)	5.69	5.75	5.80	$\pi_\perp \rightarrow$ 3s (O)

[a]MS-CAS(10e,10o)PT2/6-311+G*//MS-CAS(8e,8o)PT2/6-31+G*. [b]MS-CAS(8e,8o)PT2/6-31+G*//MS-CAS(8e,8o)PT2/6-31+G*. [c]Reference 15.

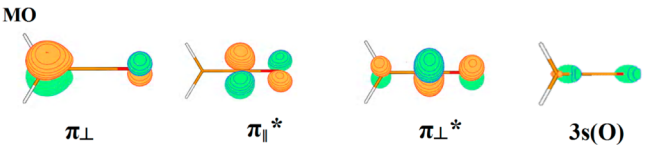

Figure 1. Frontier molecular orbitals of ketene.

3.2. Nonadiabatic Pathways. All obtained structures (GMs, LMs, TSs, MECIs, and MSXs) for the six lowest electronic states are listed in Figure 2. The corresponding PESs are described in Figure 3. Upon excitation to the S_2 state in the FC region in the wavelength range of 190−220 nm (630−544

dx.doi.org/10.1021/jp312719a | J. Phys. Chem. A 2013, 117, 7001−7008

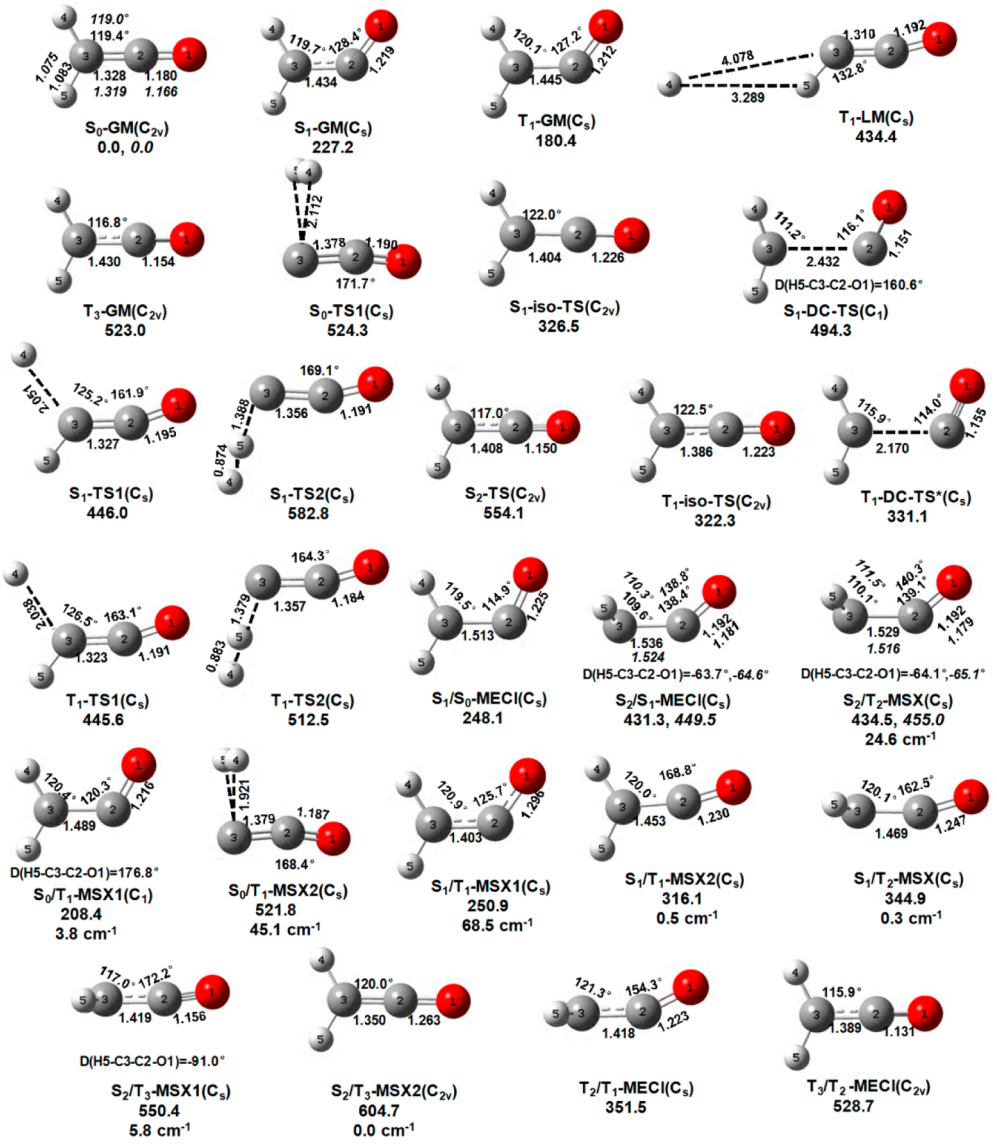

Figure 2. Optimized structures (GM, LM, TS, MECI, and MSX) involving the six lowest electronic states of ketene obtained by the MS-CAS(8e,8o)PT2/6-31+G* method, where T_1-DC-TS marked by * was optimized by single-state CASPT2 calculations due to instability in three-state calculations at these structures. Relative energy values (in kJ/mol) at corresponding levels, structure symmetry, and the spin−orbit coupling values (in cm^{-1}) between singlet and triplet states (MSXs) are shown below each structure. Geometrical parameters, bond distances (in angstroms), bond angles (in degrees), and dihedral angles (in degrees) that are relevant to the reaction mechanism are also shown. The values in italic were obtained by the MS-CAS(10e,10o)PT2/aug-cc-pVTZ method. Cartesian coordinates of all optimized geometries are listed in the Supporting Information.

kJ/mol), the ketene molecule can easily relax to S_2-TS located near the FC point maintaining the C_{2v} symmetry. The IRC from S_2-TS reduces the symmetry from C_{2v} to C_s leading to two equivalent regions involving S_2/S_1-MECI (see Figure S1 in the Supporting Information). The S_2/S_1-MECI point is the lowest energy point on the S_2 PES. In fact, there is no minimum on S_2. This is in accord with the previous proposal by Allen and Schaefer[13] that there is no minimum on the S_2 state due to conical intersections. As shown in Figure 2, S_2/S_1-MECI belongs to the C_s-I type with deviation along the symmetric out-of-plane (C_s-I) mode from the C_{2v} molecular plane. This supports the previous interpretation of the observed rotational propensity of angular anisotropy[10] assuming a molecular motion along the C_s-I mode on S_2 and/or S_1. Intriguingly, there is a seam of crossing between the S_2 and T_2 states (S_2/T_2-MSX) very close to S_2/S_1-MECI, as shown in Figure 2. The differences in angles and in bond lengths are merely less than 1.0° and 0.01 Å, respectively, and the difference in energy is just 3.2 kJ/mol. The T_2 and S_1 states in this region have the same A″ electronic configuration and nearly the same energies, whereas S_2 has an A′ configuration. Therefore, these S_2, S_1, and T_2 surfaces come very close in the same region, and this region is denoted as $S_2/S_1/T_2$ below. An IC around $S_2/S_1/T_2$ brings the system down to the S_1 PES. Subsequently, a transition to the S_0 PES can take place through the well-known S_1/S_0-MECI located in the low energy region of the S_1 PES. ISC may compete with IC in the close vicinity of singlet/triplet seams of crossing.[26] After the ISC around $S_2/S_1/T_2$ from S_2 to T_2, it would proceed via T_2/S_1-MSX to S_1 or via T_2/T_1-MECI to T_1. These T_2/S_1-MSX and T_2/T_1-MECI are located in the same region as have been reported in ref 16 and denoted $T_2/S_1/T_1$

dx.doi.org/10.1021/jp312719a | J. Phys. Chem. A 2013, 117, 7001−7008

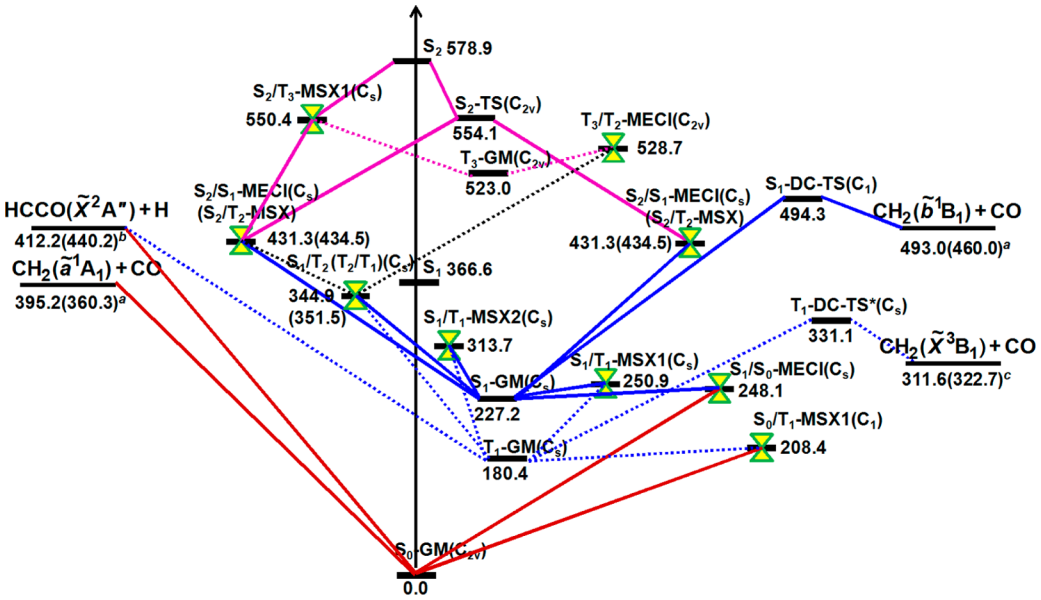

Figure 3. PESs (in kJ/mol) for the processes of ketene photoexcitation and photolysis (the corresponding structures are shown in Figure 2). Experimental dissociation energies, *a*, *b*, and *c*, from refs 40, 41, and 42, respectively, are shown in parentheses.

below. On both S_1 and T_1, the system can make a transition to S_0 either around S_1/S_0-MECI or S_0/T_1-MSX, respectively.

In the FC region on the S_2 state, an intersection between the S_2 and T_3 states (S_2/T_3-MSX1) was located. S_2/T_3-MSX1 again belongs to the C_s-I type, and the IRC from S_2-TS passes near the S_2/T_3-MSX1 region. Thus, non-negligible fraction of population can transfer to T_3 if ultrafast ISC[26] takes place around S_2/T_3-MSX1. After the ISC, the system relaxes to the T_3 minimum (T_3-GM) with C_{2v} symmetry. The series of these geometry changes would excite the vibration along the C_s-I mode, which is consistent with the observed rotational propensity of angular anisotropy.[10] Around T_3-GM there is a conical intersection between the T_3 and T_2 states (T_3/T_2-MECI). T_3/T_2-MECI can easily be reached from T_3-GM, as it is only 5.7 kJ/mol higher in energy than T_3-GM. After the IC to T_2 around T_3/T_2-MECI, the system would reach to the $T_2/S_1/T_1$ region and decay down to either S_1 or T_1.

Previously, Liu and co-workers reported an IC path from S_2 to S_1, using CAS(14e,14o)SCF/aug-cc-pVTZ for structure optimization and (SS-)CAS(14e,14o)PT2 for single point calculation, i.e., CASPT2//CASSCF.[20] There are two differences between the present CASPT2 and their CASPT2//CASSCF results. First, they found a local minimum with C_{2v} symmetry on S_2 near the FC point at the CASSCF level. However, no minimum was found on S_2 in this study as well as in the early study by Allen and Schaefer.[13] We confirmed this also at the (MS-)CAS(10e,10o)PT2/aug-cc-pVTZ level. Moreover, even in their results,[20] the S_2 minimum turned to be higher in energy than the TS connecting the minimum and the S_2/S_1-MECI region with the single-point energy evaluation by CASPT2, and this suggests that it is not a genuine minimum on S_2 at the CASPT2 level. Therefore, all the previous[13,20] and the present calculations are consistently indicating that there is no minimum on S_2. The second difference is that they suggested that there is an S_2/T_1-MSX around the S_2/S_1-MECI, instead of the S_2/T_2-MSX found in this study. This difference is crucial in discussing the efficiency of the ISC. They proposed that the ISC is prohibited due to a negligible SO-coupling 0.136 cm^{-1} between S_2 and T_1. However, the SO-coupling 24.6 cm^{-1} between S_2 and T_2 at the present S_2/T_2-MSX is substantial, as they belong to A′ and A″ electronic configuration, respectively. For confirmation, single point calculations were made at their S_2/T_1-MSX and the present S_2/T_2-MSX geometries by MS-CAS(14e,14o)PT2/aug-cc-pVTZ. The energy difference between S_2 and T_2 at the present S_2/T_2-MSX is 9.3 kJ/mol, whereas the gap between S_2 and T_1 at their S_2/T_1-MSX is 154.6 kJ/mol. Moreover, both S_2/S_1-MECI and S_2/T_2-MSX were also located at the MS-CAS(10e,10o)PT2/aug-cc-pVTZ level in the close vicinity as shown in Figure 2. Thus, at the CASPT2 level, we conclude that T_2 intersects with S_2.

In summary, five working pathways were found from the FC region on S_2 to S_0:

(A) S_2–FC → S_2-TS → $S_2/S_1/T_2$ → S_1 → S_1/S_0-MECI → S_0

(B) S_2–FC → S_2-TS → $S_2/S_1/T_2$ → T_2 → $T_2/S_1/T_1$ → S_1 → S_1/S_0-MECI → S_0

(C) S_2–FC → S_2-TS → $S_2/S_1/T_2$ → T_2 → $T_2/S_1/T_1$ → T_1 → S_0/T_1-MSX → S_0

(D) S_2–FC → S_2-TS → S_2/T_3-MSX → T_3 → T_3/T_2-MECI → $T_2/S_1/T_1$ → S_1 → S_1/S_0-MECI → S_0

(E) S_2–FC → S_2-TS → S_2/T_3-MSX → T_3 → T_3/T_2-MECI → $T_2/S_1/T_1$ → T_1 → S_0/T_1-MSX → S_0

In other words, all the six states are involved in these nonadiabatic decay processes. The lowest energy points on all high-lying states, except for T_3, are MECI or MSX points. Moreover, T_3-GM is also very close to T_3/T_2-MECI. It follows that the decay should occur very quickly to the low-lying S_1, T_1, and S_0 states, and dissociations take place almost exclusively on these low-lying states. Hence, in the following, dissociation pathways from these three low-lying states are discussed.

3.3. Dissociation into CH_2 + CO and H + HCCO. Once the system reaches the S_1 state through a series of nonadiabatic transitions, as seen in Figure 3, three paths are open on the S_1 state:

(i) a direct dissociation to $CH_2(\tilde{b}^1B_1)$ + $CO(\tilde{X}^1\Sigma^+)$ via S_1-DC-TS,

(ii) a nonadiabatic transition to S_0 through S_1/S_0-MECI, and

dx.doi.org/10.1021/jp312719a | J. Phys. Chem. A 2013, 117, 7001−7008

(iii) a nonadiabatic transition to T_1 through S_1/T_1-MSXs (S_1/T_1-MSX1 and S_1/T_1-MSX2). Although path i should be minor in view of very high energy S_1-DC-TS, it may have a certain contribution when the excitation energy is much higher than 494.3 kJ/mol because adiabatic processes with large enough excess energy are often faster than nonadiabatic processes. Paths ii and iii can energetically compete, although path iii should be relatively minor due to spin-forbidden transition.

On the S_0 PES, the molecule can directly dissociate to $CH_2(\tilde{a}^1A_1)$ + $CO(\tilde{X}^1\Sigma^+)$ and $HCCO(\tilde{X}^2A'')$ + H without barrier. On the other hand, energetically the most preferable dissociation path is a nonadiabatic one to $CH_2(\tilde{X}^3B_1)$ + $CO(\tilde{X}^1\Sigma^+)$ through S_0/T_1-MSX and T_1-DC-TS. On T_1, the most preferable adiabatic path is that to $CH_2(\tilde{X}^3B_1)$ + $CO(\tilde{X}^1\Sigma^+)$ via T_1-DC-TS, although population of T_1 seems not to be very high because of an efficient ISC to S_0 through the very low energy S_0/T_1-MSX. Transitions between S_0 and T_1 as well as dissociation to $CH_2(\tilde{X}^3B_1)$ + $CO(\tilde{X}^1\Sigma^+)$ through T_1-DC-TS also have been discussed in previous papers.[16,21−25]

It is not easy to estimate which of the channels $CH_2(\tilde{a}^1A_1)$ + $CO(\tilde{X}^1\Sigma^+)$ and $CH_2(\tilde{X}^3B_1)$ + $CO(\tilde{X}^1\Sigma^+)$ is dominant at a given excess energy, based only on the present results. Energetically, the $CH_2(\tilde{X}^3B_1)$ + $CO(\tilde{X}^1\Sigma^+)$ channel is preferable. In other words, $CH_2(\tilde{X}^3B_1)$ is expected to be a major product at low photoexcitation energy especially when the excess energy is not enough to reach $CH_2(\tilde{a}^1A_1)$ + $CO(\tilde{X}^1\Sigma^+)$. On the other hand, in general, adiabatic processes are faster when the excess energy is much larger than the corresponding dissociation barrier. Thus $CH_2(\tilde{a}^1A_1)$ can be a major product from S_0 at high photon energy. In this case, the path to $HCCO(\tilde{X}^2A'')$ + H on S_0 would compete and $CH_2(\tilde{X}^3B_1)$ may be a minor product. The observed branching ratio in 193.3 nm photolysis by Fockenberg well corresponds to the latter situation: 66% for $^1CH_2$ + CO, 17% for HCCO + H, and 6% for $^3CH_2$ + CO.[11] Although a different trend was observed at the same wavelength in an earlier experiment,[6] it was interpreted to be not very accurate due to experimental conditions.[11] Theoretical prediction of excitation energy dependence of the branching ratios is a challenging subject. This can be achieved via surface hopping trajectory simulations either on ab initio or on fitted PESs.[26,43,44] To run a large number of trajectories efficiently, fitted analytical PESs are preferred.[45−47] In construction of such PESs, information of energetically accessible stationary structures obtained in this study will be helpful in confining sampling regions and in calibrating fitted PESs.

To further characterize the CH_2 + CO dissociation path, an MEPX was computed starting from a partially dissociated structure, at the single-state CAS(8e,8o)PT2/6-31+G* level. MEPX is the mass-weighted steepest descent path within the seam of crossing hyperspace between two surfaces. Figure 4 shows energy profiles of the S_0 and T_1 PESs along the MEPX. As seen in this figure, the crossing seam is not confined around the S_0/T_1-MSX1. In other words, during the dissociation dynamics, the S_0/T_1 transition can take place not only around S_0/T_1-MSX1 with the short C−C bond but also at longer C−C bond distances.

3.4. Dissociation into C_2O + H_2. Pathway 5, giving C_2O + H_2 products, has been suggested as a minor pathway experimentally.[6,11] For this path, mechanisms similar to those for H_2CO might be expected. In unimolecular decomposition of H_2CO to CO + H_2, two different pathways are known on the

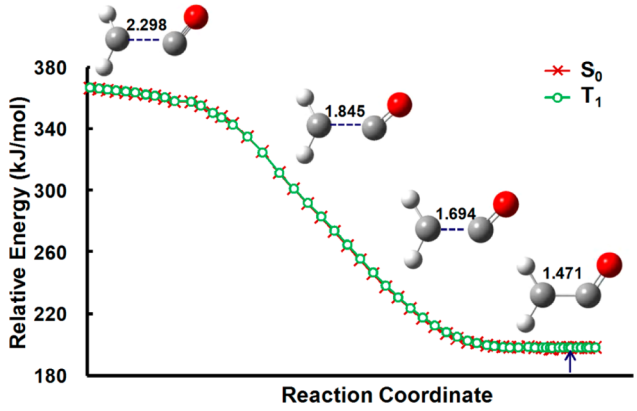

Figure 4. Minimum energy path MEPX along the S_0/T_1 crossing seam starting from a partial C−C dissociation structure, calculated at the single-state CAS(8e,8o)PT2/6-31+G* level. The energy is relative to S_0-GM at the same level. The energy difference between the two states does not exceed 1 kJ/mol along the determined MEPX.

S_0 PES. One, sometimes called the straight path, passes through a well characterized tight TS, which has been investigated in a number of theoretical studies since its discovery in 1974.[48] The other identified recently in H_2CO photolysis is called the roaming path and undergoes intramolecular recombination between HCO and H radicals.[49−51] Very recently, the roaming path was found to take place also on electronic excited states in the unimolecular decomposition of NO_3.[52−57] Thus, it is interesting to search for decomposition pathways to C_2O + H_2 thoroughly.

We explored both straight and roaming-like intramolecular recombination pathways systematically by ADDF and AFIR, respectively, on the three low-lying states, S_0, S_1, and T_1. Figure 5 illustrates energy profiles of all obtained pathways, where

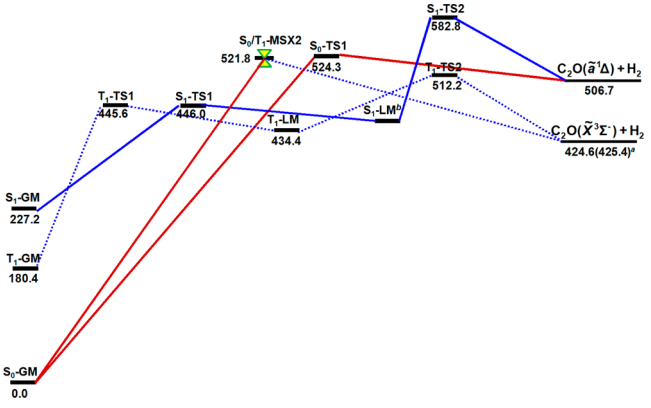

Figure 5. Pathways of ketene photodissociation into C_2O + H_2 (the corresponding structures are shown in Figure 2). Energy values are in kJ/mol. [a]The thermodynamic threshold is from refs 41 and 58. [b]Not found due to instability in the CASPT2 calculations.

corresponding stationary structures are seen in Figure 2. Energetically, the most preferable one is a roaming-like path on the T_1 PES, in which one of H atoms at first partially dissociates through T_1-TS1, then migrates around the HCCO radical, and finally abstracts the other H atom via T_1-TS2. However, this path is highly unlikely to proceed. This is because, from T_1-GM, the much faster direct dissociation to H + HCCO without barrier will complete against the intramolecular recombination. In contrast, the barrier for intramolecular recombination in

dx.doi.org/10.1021/jp312719a | J. Phys. Chem. A 2013, 117, 7001−7008

H···HCO → CO + H_2 is slightly lower than the dissociation energy to H + HCO. The excited-state roaming-like path on S_1 has a very high second barrier S_1-TS2. Obviously, on the S_0 PES, the roaming-like path is impossible to take place because $CH_2(\tilde{a}^1A_1)$ + $CO(\tilde{X}^1\Sigma^+)$ is higher in energy than HCCO-$(\tilde{X}^2A'')$ + H. Thus, roaming-like intramolecular recombination would not take place in unimolecular decomposition of ketene.

A straight path on S_0 through S_0-TS1 is open as a very minor channel when the excess energy is larger than this barrier. This path generates a product $C_2O(\tilde{a}^1\Delta)$ in an electronic excited state. Interestingly, the most stable, triplet product $C_2O(\tilde{X}^3\Sigma^-)$ can be produced from S_0 with a nonadiabatic transition via S_0/T_1-MSX2. These two pathways from S_0 may compete with each other with similar barriers. In other words, both the singlet and triplet products may be generated from S_0 either by adiabatic or nonadiabatic process. These two pathways explain the observed minor C_2O product.

4. CONCLUSIONS

In this study, critical structures, i.e., GMs, LMs, TSs, MECIs, and MSXs, on and between the six lowest electronic states of ketene were explored systematically at the CASPT2 level, by using the GRRM/ADDF and GRRM/AFIR strategies. On the basis of the energetics obtained in the exploration, photodissociation mechanisms of ketene from S_2 were discussed in detail. We located five unique nonadiabatic decay pathways from S_2 to the low-lying S_1, T_1, and S_0.

(A) S_2−FC → S_2-TS → $S_2/S_1/T_2$ → S_1 → S_1/S_0-MECI → S_0
(B) S_2−FC → S_2-TS → $S_2/S_1/T_2$ → T_2 → $T_2/S_1/T_1$ → S_1 → S_1/S_0-MECI → S_0
(C) S_2−FC → S_2-TS → $S_2/S_1/T_2$ → T_2 → $T_2/S_1/T_1$ → T_1 → S_0/T_1-MSX → S_0
(D) S_2−FC → S_2-TS → S_2/T_3-MSX → T_3 → T_3/T_2-MECI → $T_2/S_1/T_1$ → S_1 → S_1/S_0-MECI → S_0
(E) S_2−FC → S_2-TS → S_2/T_3-MSX → T_3 → T_3/T_2-MECI → $T_2/S_1/T_1$ → T_1 → S_0/T_1-MSX → S_0

Because the PES is almost always downhill entirely along these five pathways, ketene is expected to reach these low-lying states very quickly. On S_1, T_1, and S_0, five dissociation channels 1−5 are open.

$$H_2CCO + h\nu \rightarrow CH_2(\tilde{X}^3B_1) + CO \quad (1)$$

$$CH_2(\tilde{a}^1A_1) + CO \quad (2)$$

$$CH_2(\tilde{b}^1B_1) + CO \quad (3)$$

$$HCCO(\tilde{X}^2A'') + H \quad (4)$$

$$C_2O + H_2 \quad (5)$$

The CH_2 product via channels 1−3 can be produced from all the three S_1, T_1, and S_0 states, and the T_1 path is energetically the most preferable. Dissociation on S_0 can compete with the T_1 path depending on the excess energy. We located a wide S_0/T_1 seam along the CH_2 dissociation coordinate, which could play a key role in determining the branching ratio between the S_0 and T_1 pathways. For obtaining the excess energy dependence of the branching ratio, further dynamical studies are required in the future. In addition to these three CH_2 dissociation channels, dissociation pathways of the H atom, channel 4, and H_2 molecule, channel 5, were also located and discussed. H atoms can be generated from both S_0 and T_1 as corresponding dissociation limits are identical between these two states. The H_2 molecule can be generated exclusively from S_0 via either adiabatic or nonadiabatic processes. The adiabatic path produces the higher energy singlet CCO molecule, whereas in the nonadiabatic path the most stable triplet CCO molecule is generated. The present study provides a comprehensive view of complex unimolecular photoreactions of ketene involving multiple channels and will be useful in interpretation of and in understanding results of future experiments and dynamical simulations.

■ ASSOCIATED CONTENT

Supporting Information

IRC curves of S_2-TS in Figure S1 and Cartesian coordinates of all the structures in Figure 2. This material is available free of charge via the Internet http://pubs.acs.org.

■ AUTHOR INFORMATION

Corresponding Author

*E-mail: S.M., smaeda@mail.sci.hokudai.ac.jp; K.M., morokuma@fukui.kyoto-u.ac.jp.

Notes

The authors declare no competing financial interest.

■ ACKNOWLEDGMENTS

The authors thank Dr. Fengyi Liu and Dr. Lung Wa Chung for their helpful discussions on excited-state calculations. This work is partly supported by a grant from Japan Science and Technology Agency with a Core Research for Evolutional Science and Technology (CREST) in the Area of High Performance Computing for Multiscale and Multiphysics Phenomena at Kyoto University, grants from Japan Society for the Promotion of Science (Grants-in-Aid for Scientific Research <KAKENHI> No. 23685004 at Hokkaido University and No. 24245005 at Kyoto University), and a grant from US AFOSR (Grant No. FA9550-10-1-0304) at Emory University.

■ REFERENCES

(1) Chen, I.-C.; Green, W. H., Jr.; Moore, C. B. Bond Breaking without Barriers: Photofragmentation of Ketene at the Singlet Threshold. *J. Chem. Phys.* **1988**, *89*, 314−328.
(2) (a) Chen, I.-C.; Moore, C. B. Photofragmentation of Ketene to $CH_2(\tilde{X}^3B_1)$ + CO. 1. Barrier Height and Dissociation Rate Constant. *J. Phys. Chem.* **1990**, *94*, 263−269. (b) Chen, I.-C.; Moore, C. B. Photofragmentation of Ketene to $CH_2(\tilde{X}^3B_1)$ + CO. 2. Rotational-State Distributions of Product CO. *J. Phys. Chem.* **1990**, *94*, 269−274.
(3) Kim, S. K.; Choi, Y. S.; Pibel, C. D.; Zheng, Q. K.; Moore, C. B. Determination of the Singlet/Triplet Branching Ratio in the Photodissociation of Ketene. *J. Chem. Phys.* **1991**, *94*, 1954−1960.
(4) Lovejoy, E. R.; Kim, S. K.; Moore, C. B. Observation of Transition-State Vibrational Thresholds in the Rate of Dissociation of Ketene. *Science* **1992**, *256*, 1541−1544.
(5) Liu, X.; Westre, S. G.; Getty, J. D.; Kelly, P. B. Examination of the Ketene $^1B_1$ State Photodissociation Dynamics by Far-Ultraviolet Resonance Raman Spectroscopy. *Chem. Phys. Lett.* **1992**, *188*, 42−48.
(6) Moreno, I. G.; Lovejoy, E. R.; Moore, C. B. Photodissociation of Ketene: Vibrationally Excited $CH_2(\tilde{a}^1A_1)$. *J. Chem. Phys.* **1994**, *100*, 8902−8906.
(7) Kim, S. K.; Lovejoy, E. R.; Moore, C. B. Transition State Vibrational Level Thresholds for the Dissociation of Triplet Ketene. *J. Chem. Phys.* **1995**, *102*, 3202−3219.
(8) Glass, G. P.; Kumaran, S. S.; Michael, J. V. Photolysis of Ketene at 193 nm and the Rate Constant for H + HCCO at 297 K. *J. Phys. Chem. A* **2000**, *104*, 8360−8367.
(9) Feltham, E. J.; Qadiri, R. H.; Cottrill, E. E. H.; Cook, P. A.; Cole, J. P.; Balint-Kurti, G. G.; Ashfold, M. N. R. Ketene Photodissociation

in the Wavelength Range 193-215 nm: The H Atom Production Channel. *J. Chem. Phys.* **2003**, *119*, 6017−6031.
(10) Liu, J.; Wang, F. Y.; Wang, H.; Jiang, B.; Yang, X. M. A Velocity Map Ion-Imaging Study on Ketene Photodissociation at 208 and 213 nm: Rotational Dependence of Product Angular Anisotropy. *J. Chem. Phys.* **2005**, *122*, 104309(1−6).
(11) Fockenberg, C. Product Study of the Photolysis of Ketene and Ethyl Ethynyl Ether at 193.3 nm. *J. Phys. Chem. A* **2005**, *109*, 7140−7150.
(12) Yamabe, S.; Morokuma, K. A Theoretical Study on the Paths of Photodissociation: $CH_2{=}C{=}O \rightarrow CH_2 + CO$. *J. Am. Chem. Soc.* **1978**, *100*, 7551−7556.
(13) Allen, W. D.; Schaefer, H. F., III. Ab Initio Studies of the Low-Lying Electronic States of Ketene. *J. Chem. Phys.* **1986**, *84*, 2212−2225.
(14) Allen, W. D.; Schaefer, H. F., III. Reaction Paths for the Dissociation $\tilde{a}^3A''CH_2CO \rightarrow \tilde{X}^3B_1CH_2 + \tilde{X}^1\Sigma^+CO$. *J. Chem. Phys.* **1988**, *89*, 329−344.
(15) Szalay, P. G.; Császár, A. G.; Nemes, L. Electronic States of Ketene. *J. Chem. Phys.* **1996**, *105*, 1034−1045.
(16) Cui, Q.; Morokuma, K. Ab Initio Study of Nonadiabatic Interactions in the Photodissociation of Ketene. *J. Chem. Phys.* **1997**, *107*, 4951−4959.
(17) Yarkony, D. R. S_1-S_0 Internal Conversion in Ketene. 1. The Role of Conical Intersections. *J. Phys. Chem. A* **1999**, *103*, 6658−6668.
(18) Forsythe, K. M.; Gray, S. K.; Klippenstein, S. J.; Hall, G. E. An Ab Initio Molecular Dynamics Study of S_0 Ketene Fragmentation. *J. Chem. Phys.* **2001**, *115*, 2134−2145.
(19) Cole, J. P.; Balint-Kurti, G. G. A Statistical, Ab Initio, Quantum Mechanical Study of the Photolysis and Final State Distributions of Singlet Ketene. *J. Chem. Phys.* **2003**, *119*, 6003−6016.
(20) Liu, Y.; Yu, J. K.; Huang, X. R.; Sun, C. C. Theoretical Study of Photodissociation Dynamics on the Lowest-Lying Rydberg State of Ketene. *J. Chem. Phys.* **2006**, *125*, 044311(1−5).
(21) Klippenstein, S. J.; East, A. L. L.; Allen, W. D. A High Level Ab Initio Map and Direct Statistical Treatment of the Fragmentation of Singlet Ketene. *J. Chem. Phys.* **1996**, *105*, 118−140.
(22) Kaledin, A. L.; Seong, J.; Morokuma, K. Predominance of Nonequilibrium Dynamics in the Photodissociation of Ketene in the Triplet State. *J. Phys. Chem. A* **2001**, *105*, 2731−2737.
(23) Ogihara, Y.; Yamamoto, T.; Kato, S. Quantum Mechanical Reaction Probability of Triplet Ketene at the Multireference Second-Order Perturbation Level of Theory. *J. Phys. Chem. A* **2010**, *114*, 9981−9990.
(24) Ogihara, Y.; Yamamoto, T.; Kato, S. Multireference Coupled-Cluster Calculation of the Dissociation Energy Profile of Triplet Ketene. *Chem. Phys. Lett.* **2011**, *511*, 28−32.
(25) Ogihara, Y.; Yamamoto, T.; Kato, S. Ab Initio Trajectory Study on Triplet Ketene Photodissociation via Statistical Sampling of the Crossing Seam. *J. Chem. Theory Comput.* **2011**, *7*, 2507−2519.
(26) Richter, M.; Marquetand, P.; González-Vázquez, J.; Sola, I.; González, L. Femtosecond Intersystem Crossing in the DNA Nucleobase Cytosine. *J. Phys. Chem. Lett.* **2012**, *3*, 3090−3095.
(27) Maeda, S.; Ohno, K.; Morokuma, K. Automated Global Mapping of Minimal Energy Points on Seams of Crossing by the Anharmonic Downward Distortion Following Method: A Case Study of H_2CO. *J. Phys. Chem. A* **2009**, *113*, 1704−1710.
(28) Ohno, K.; Maeda, S. A Scaled Hypersphere Search Method for the Topography of Reaction Pathways on the Potential Energy Surface. *Chem. Phys. Lett.* **2004**, *384*, 277−282.
(29) Maeda, S.; Ohno, K. Global Mapping of Equilibrium and Transition Structures on Potential Energy Surfaces by the Scaled Hypersphere Search Method: Applications to Ab Initio Surfaces of Formaldehyde and Propyne Molecules. *J. Phys. Chem. A* **2005**, *109*, 5742−5753.
(30) Ohno, K.; Maeda, S. Global Reaction Route Mapping on Potential Energy Surfaces of Formaldehyde, Formic Acid, and Their Metal-Substituted Analogues. *J. Phys. Chem. A* **2006**, *110*, 8933−8941.
(31) Maeda, S.; Ohno, K.; Morokuma, K. Exploring Multiple Potential Energy Surfaces: Photochemistry of Small Carbonyl Compounds. *Adv. Phys. Chem.* **2012**, *2012*, 268124/1−13.
(32) Maeda, S.; Morokuma, K. Finding Reaction Pathways of Type A + B → X: Toward Systematic Prediction of Reaction Mechanisms. *J. Chem. Theory Comput.* **2011**, *7*, 2335−2345.
(33) Bearpark, M. J.; Robb, M. A.; Schlegel, H. B. A Direct Method for the Location of the Lowest Energy Point on A Potential Surface Crossing. *Chem. Phys. Lett.* **1994**, *223*, 269−274.
(34) Maeda, S.; Ohno, K.; Morokuma, K. Updated Branching Plane for Finding Conical Intersections without Coupling Derivative Vectors. *J. Chem. Theory Comput.* **2010**, *6*, 1538−1545.
(35) *GRRM*, a developmental version. Maeda, S.; Osada, Y.; Morokuma, K.; Ohno, K.
(36) *MOLPRO*, Versions 2006.1 and 2008.1, A Package of Ab Initio Programs. Werner, H.-J.; Knowles, P. J.; Lindh, R.; Manby, F. R.; Schütz, M.; Celani, P.; Korona, T.; Mitrushenkov, A.; Rauhut, G.; Adler T. B.; et al. See http://www.molpro.net.
(37) Roos, B. O.; Andersson, K. Multiconfigurational Perturbation Theory with Level Shift − the Cr_2 Potential Revisited. *Chem. Phys. Lett.* **1995**, *245*, 215−223.
(38) *MOLPRO*, Version 2010.1, A Package of Ab Initio Programs. Werner, H.-J.; Knowles, P. J.; Lindh, R.; Manby, F. R.; Schütz, M.; Celani, P.; Korona, T.; Mitrushenkov, A.; Rauhut, G.; Adler, T. B.; et al. See http://www.molpro.net.
(39) Aquilante, F.; De Vico, L.; Ferre, N.; Ghigo, G.; Malmqvist, P.-Å; Neogrady, P.; Pedersen, T. B.; Pitonak, M.; Reiher, M.; Roos, B. O.; et al. MOLCAS 7: The Next Generation. *J. Comput. Chem.* **2010**, *31*, 224−247.
(40) Moore, C. B. Spiers Memorial Lecture State-resolved Studies of Unimolecular Reactions. *Faraday Discuss.* **1995**, *102*, 1−15.
(41) Berkowitz, J.; Ellison, G. B.; Gutman, D. Three Methods to Measure RH Bond Energies. *J. Phys. Chem.* **1994**, *98*, 2744−2765.
(42) Jacox, M. E. Vibrational and Electronic Energy Levels of Polyatomic Transient Molecules: Supplement 1. *J. Phys. Chem. Ref. Data* **1990**, *19*, 1387−1546.
(43) Fu, B.; Shepler, B. C.; Bowman, J. M. Three-State Trajectory Surface Hopping Studies of the Photodissociation Dynamics of Formaldehyde on Ab Initio Potential Energy Surfaces. *J. Am. Chem. Soc.* **2011**, *133*, 7957−7968.
(44) Tully, J. C. Perspective: Nonadiabatic Dynamics Theory. *J. Chem. Phys.* **2012**, *137*, 22A301−7.
(45) Braams, B. J.; Bowman, J. M. Permutationally Invariant Potential Energy Surfaces in High Dimensionality. *Int. Rev. Phys. Chem.* **2009**, *28*, 577−606.
(46) Bowman, J. M.; Braams, B. J.; Carter, S.; Chen, C.; Czakó, G.; Fu, B.; Huang, X.; Kamarchik, E.; Sharma, A. R.; Shepler, B. C.; et al. Ab-Initio-Based Potential Energy Surfaces for Complex Molecules and Molecular Complexes. *J. Phys. Chem. Lett.* **2010**, *1*, 1866−1874.
(47) Bowman, J. M.; Czakó, G.; Fu, B. High-Dimensional Ab Initio Potential Energy Surfaces for Reaction Dynamics Calculations. *Phys. Chem. Chem. Phys.* **2011**, *13*, 8094−8111.
(48) Jaffe, R. L.; Hayes, D. M.; Morokuma, K. Photodissociation of Formaldehyde: Potential Energy Surfaces for $H_2CO \rightarrow H_2 + CO$. *J. Chem. Phys.* **1974**, *60*, 5108−5109.
(49) Townsend, D.; Lahankar, S. A.; Lee, S. K.; Chambreau, S. D.; Suits, A. G.; Zhang, X.; Rheinecker, J.; Harding, L. B.; Bowman, J. M. The Roaming Atom: Straying from the Reaction Path in Formaldehyde Decomposition. *Science* **2004**, *306*, 1158−1161.
(50) Herath, N.; Suits, A. G. Roaming Radical Reactions. *J. Phys. Chem. Lett.* **2011**, *2*, 642−647.
(51) Bowman, J. M.; Shepler, B. C. Roaming Radicals. *Annu. Rev. Phys. Chem.* **2011**, *62*, 531−553.
(52) Xiao, H.-Y.; Maeda, S.; Morokuma, K. Excited State Roaming Dynamics in Photolysis of Nitrate Radical. *J. Phys. Chem. Lett.* **2011**, *2*, 934−938.
(53) North, S. W. Roaming in the Dark. *Nat. Chem.* **2011**, *3*, 504−505.

(54) Grubb, M. P.; Warter, M. L.; Xiao, H.-Y.; Maeda, S.; Morokuma, K.; North, S. W. No Straight Path: Roaming in Both Ground- and Excited-State Photolytic Channels of $NO_3 \rightarrow NO + O_2$. *Science* **2012**, *335*, 1075−1078.
(55) Grubb, M. P.; Warter, M. L.; North, S. W. Stereodynamics of Multistate Roaming. *Phys. Chem. Chem. Phys.* **2012**, *14*, 6733−6740.
(56) Xiao, H.-Y; Maeda, S.; Morokuma, K. Global Ab Initio Potential Energy Surfaces for Low-Lying Doublet States of NO_3. *J. Chem. Theory. Comput.* **2012**, *8*, 2600−2605.
(57) Fu, B.; Bowman, J. M.; Xiao, H.-Y; Maeda, S.; Morokuma, K. Quasiclassical Trajectory Studies of the Photodissociation Dynamics of NO_3 from the D_0 and D_1 Potential Energy Surfaces. *J. Chem. Theory. Comput.* **2013**, *9*, 893−900.
(58) Choi, H.; Mordaunt, D. H.; Bise, R. T.; Taylor, T. R.; Neumark, D. M. Photodissociation of Triplet and Singlet States of the CCO Radical. *J. Chem. Phys.* **1998**, *108*, 4070−4078.